COMPACT CORE GALAXIES IN THE RESOLVE SURVEY

Elaine M. Snyder[1], Sheila J. Kannappan[1], Dara J. Norman[2], Mark N. Norris[3], Callie Hood[1], Ashley S. Bittner[1], Kathleen D. Eckert[1], Amanda J. Moffett[1,4], David V. Stark[1], and the RESOLVE Team

[1]Department of Physics and Astronomy, University of North Carolina, 141 Chapman Hall CB 3255, Chapel Hill, NC 27599, USA; emsnyder@live.unc.edu
[2]National Optical Astronomical Observatory, 950 N Cherry Ave, Tucson, AZ 85719, USA
[3]Jeremiah Horrocks Institute, University of Central Lancashire, Preston, PR1 2HE, United Kingdom and
[4]International Centre for Radio Astronomy Research (ICRAR), The University ofWestern Australia, 35 Stirling High- way, Crawley, WA 6009, Australia
Draft version April 18, 2016

ABSTRACT

We analyze the complete set of 96 compact core galaxies (CCGs) in the volume-limited RESOLVE survey to investigate the formation and evolution of compact galaxies such as ultra compact dwarfs (UCDs), compact ellipticals (cEs), and dwarf ellipticals (dEs) across a broad statistical distribution of environments. We perform one and two component Sérsic fits KIDSS for all galaxies in the RESOLVE sample with UKIDSS Y-band imaging using GALFIT, which produces seeing-deconvolved effective radius (R_{eff}) measurements. The one component fits are used to select candidate CCGs with $R_{eff} < 1000$ pc, and then perform new two component fits to these galaxies with the Sérsic n of the second component held fixed at 1 for an exponential disk. We finalize the CCG sample by selecting on core-only (first component) $R_{eff} < 800$pc, an upper limit that encompasses all of the similarly compact stellar systems (UCDs, cEs, dEs) included in the Archive of Intermediate Mass Stellar Systems (AIMSS) catalog. We quantify the amount of light in the core and envelope of each CCG by taking the logarithm of the ratio of the fluxes in each component. The result is a smooth continuum of CCGs that range from envelope-dominated to core+envelope to core-dominated. With GALEX *NUV*, SDSS *ugriz*, and 2MASS/UKIDSS *YJHK* data, we derive colors and star formation histories and find that a significant number of CCGs live on the blue sequence and have recently formed stars. We find that CCGs naturally occur in a range of environments from isolated to cluster. We compare velocity dispersions of CCGs derived from Gemini IFU data and SOAR spectroscopy to velocity dispersions of other RESOLVE galaxies and the cEs and and dEs of AIMSS. We search for CCGs offset to higher or lower dispersion in the dispersion-stellar mass relation, which may indicate tidal stripping or dissipative formation, respectively. Initial results show several CCGs following the dissipative formation track.

Keywords: galaxies: formation, evolution — surveys

1. INTRODUCTION

The term compact stellar system (CSS) encompasses a class of galaxies that spans the radius range ($\sim 10-800$ pc), lying between globular clusters (GCs) and normal elliptical galaxies (Es). Different types of CSSs include ultra compact dwarf galaxies (UCDs; Phillipps et al. (2001)), compact elliptical galaxies (cEs; Faber (1973)), dwarf elliptical galaxies (dEs), and nucleated dwarf elliptical galaxies (dE,Ns). There are many unanswered questions about CSSs, typically involving how they form and evolve through time. One fact that makes the study of these compact galaxies so intriguing is their relative scarcity, which raises the question as to whether they are an intermediate and short-lived evolutionary phase in the life of a galaxy, or simply hard to find due to their size. Only in the last 15 years have we discovered enough (~ 40) of these objects to enable studies of their formation scenarios and evolution over cosmic time.

UCDs, the smallest of the CSSs mentioned above with radii ranging from 10–100 pc (see Figure 11 in Norris et al. (2014)), are largely believed to be either the high mass extension of the globular cluster population (Drinkwater et al. (2000), Mieske et al. (2002)) or tidally-stripped remnants of nucleated dwarf galaxies (Bekki et al. (2001), Bekki & Freeman (2003), Jennings et al. (2015), Zhang et al. (2015)). Norris & Kannappan (2011) find evidence that UCDs are a "mixed bag" of both giant GCs and stripped nuclei based on their analysis of UCDs discovered near the elliptical galaxy NGC3923 and S0 galaxy NGC4546. Seth et al. (2014) find a

supermassive black hole at the center of a UCD near M60, a massive elliptical galaxy, lending more evidence toward tidal stripping being a common for UCDs.

Meanwhile, cEs have radii ranging typically from ∼100–600 pc (again see Figure 11 in Norris et al. (2014)). They are typically thought to be either the result of a tidal stripping event, as is the case for the prototypical cE, M32 (Choi et al. (2002), Graham (2002)), or as a part of the low mass extension to the E population. The evidence for tidal stripping includes finding tidal streams near cEs (Smith Castelli et al. (2008), Chilingarian et al. (2009)) and one cE, studied in Kormendy et al. (1997), that is believed to host a central massive black hole. On the other hand, Kormendy & Bender (2012) argue that cEs are the extension of normal E galaxies.

dEs and their nucleated counterparts, dE,Ns, are the largest of the CSSs mentioned with radii ranging from ∼600-800 pc (again see Figure 11 in Norris et al. (2014)). Similarly to cEs, dEs and dE,Ns are thought to be either tidally stripped remnants (Crnojević et al. (2014) find dEs in M31 that show signs of tidal stripping) or the low mass extension to elliptical galaxies (Crawford et al. 2016). They could also be the remnants of LCBDs that have been ram-pressure stripped as they entered the cluster environment and subsequently quenched. There is some evidence that dE,Ns are the progenitors of UCDs (Pfeffer & Baumgardt (2013), Zhang et al. (2015), Liu et al. (2015)).

Clues to how a CSS is formed may be given by their environments. UCDs, cEs, dEs have all been found in clus-

ters (for UCDs: Price et al. (2009), Madrid et al. (2010), Haşegan et al. (2005), Jones et al. (2006), Mieske et al. (2009), Wehner & Harris (2007), Misgeld et al. (2008); for cEs: Chilingarian et al. (2007), Smith Castelli et al. (2012), Price et al. (2009); and dEs: (Smith Castelli et al. 2012), Koo et al. (1994), Guzmán et al. (1996), Crawford et al. (2016)). Fewer CSSs have been found in groups: Evstigneeva et al. (2007) find one definite UCD and two candidates in the Dorado group as well as two candidates in the NGC1400 group and Hau et al. (2009) find a UCD near the Sombrero galaxy; Huxor et al. (2011) and Chilingarian & Bergond (2010) find cEs in groups; and Crnojeviăă et al. (2014) Penny et al. (2014) find dEs in groups. Lastly, only cEs have been found in isolated environments: Huxor et al. (2013), Paudel et al. (2014), and Chilingarian & Zolotukhin (2015) find cEs separated from other galaxies by > 1 Mpc.

Given the similarities in formation scenarios and environments for these CSSs, we propose to study these galaxies as a part of a continuum of compact galaxies instead of being broken up into (perhaps somewhat arbitrary) classes based on R_{eff}. Critical to this study is a ubiquitous sample of CSSs that will allow us to analyze their formation as a function of all environments. Previous studies have mainly focused on selecting targets in the group/cluster environments, since this route is often more convenient. Our goal is thus to create a complete and volume-limited sample of compact galaxies across all environments so that we may examine their formation and evolution.

This paper presents the preliminary results of this work, characterizing the colors, star formation histories, environments, and preliminary kinematics of the first complete, volume-limited sample of CCGs. The paper is organized as follows. We explain our methods for performing seeing-deconvolved one and two component fits for the entire RESOLVE sample using GALFIT in § 2.3.1. We then explain the selection of the CCG sample from the RESOLVE survey in § 2.3.2. We then describe our photometric and spectroscopic data and analysis in § 3. We gives our results in § 4. Lastly, our results are summarized in § 5.

2. SAMPLES

2.1. *The RESOLVE survey*

We use the RESOLVE survey (Kannpann & Wei 2008, Kannappan et al., in prep) as the parent sample for our census of CCGs. RESOLVE is ideal because it is an unusually complete and volume-limited survey, which allows us to find CCGs at all evolutionary stages. RESOLVE falls within the footprint of the Sloan Digital Sky Survey (SDSS, York et al. (2000)), and is designed to span two individual semesters: A for the spring sky and B for the fall, which overlaps much of Stripe-82. RESOLVE-A spans $\sim 38,400$ Mpc^3 and occupies the region $131.25° < RA < 236.25°$, $0° < Dec < 5°$, and 4500 km s$^{-1} < cz < 7000$ km s^{-1}, while RESOLVE-B spans $\sim 13,7000$ Mpc^3 and occupies the region $330° < RA < 45°$, $-1.25° < Dec < 1.255°$, and 4500 km s$^{-1} < cz < 7000$ km s^{-1}.

RESOLVE's exceptional completeness is due to our use of multiple redshift surveys to recover galaxies that were missed in SDSS due to fiber collisions and several issues with their photometry pipeline. These issues include the oversubtraction of sky around galaxies that causes their flux to be underestimated and thereby not meet the magnitude cut for spectroscopic follow-up; the "shredding" of galaxies in which the pipeline breaks up a single galaxy into individual pieces, mak-

ing no one piece meet the magnitude cut; and the intentional exclusion of low surface brightness galaxies ($\mu_{50} < 24.5$ mag arcsec^{-2}), even if they meet the magnitude cut. We have used SDSS along with additional redshifts from archival sources (the Updated Zwicky Catalog (Falco et al. 1999), HyperLeda (Paturel et al. 2003), 6dF (Jones et al. 2009), 2dF (Colless et al. 2001), GAMA (Driver et al. 2011), and ALFALFA (Haynes et al. 2011)) to counteract these issues and build up the survey's membership.

With its improved redshift recovery, RESOLVE is complete down to absolute *r*-band magnitudes of -17.33 and -17.0 for the A and B semesters, respectively. We can convert these absolute magnitude limits into stellar mass limits: $M_\star \sim 10^{8.9}$ M$_\odot$ for the A semester and $M_\star \sim 10^{8.7}$ M$_\odot$ in the B semester (see Figure 7 in Eckert et al. (2016)). In Figure 1, we plot the stellar masses against the deconvolved R_{eff} (see § 2.3.1) and see that these limits allow us to reach down to CSSs with sizes similar to cEs. We are not able to recover UCD-like objects, but this should not matter since we are studying CSSs as a whole in order to investiage evolutionary sequences.

An important caveat to RESOLVE's completeness is that the survey is most likely to be missing the objects this study is focused on, cEs. This is because these objects can often be mistaken for stars in redshift surveys using tools such as the `class_star` parameter in Source Extractor (Bertin & Arnouts 1996), which uses the flux and ellipticity of an object to determine the probability of it being a star or a galaxy. There are current ongoing efforts to use photo-z estimates to recover these objects.

2.2. *The AIMSS catalog*

We use the Archive of Intermediate Mass Stellar Systems (AIMSS) catalog (Norris et al. (2014), Forbes et al. (2014), Janz et al. (2015)) as a reference sample for our CCGs. AIMSS is a catalog of spectroscopically confirmed CSSs found in groups and clusters and includes both literature and newly discovered objects. Their process to find new CSSs is as follows. First, a search is conducted in the Hyperleda redshift catalog (Paturel et al. 2003) for all galaxies at distances between ~ 7 and 200 Mpc (to ensure CSSs with $R_{eff} > 50$ pc will be resolved in any available HST imaging) and with $M_B < -15$. Once complete, the team then searches the Hubble Space Telescope archive for WFCP2, ACS, and WFC3 imaging within 150kpc in projection of the selected galaxies. Next, Source Extractor is run on the HST images, and candidates are identified using a training set of previously known CSSs from the literature. Once cross-matched to ensure none are previously known and vetted by eye, spectra are obtained, redshift confirmation is performed, and velocity dispersions are extracted. AIMSS also includes literature data for other UCDs, cEs, (nucleated) dEs, dwarf spheroidals, dwarf S0s, young massive clusters, and Es. AIMSS compiles M_V, stellar mass, effective radius, and velocity dispersions for each of its objects. Thus, though not a statistically-defined sample, AIMSS provides a useful reference catalog to which we can calibrate and compare our CCGs.

2.3. *CCG sample selection*

2.3.1. *Deconvolution of RESOLVE galaxies*

We begin our analysis by deriving seeing-deconvolved R_{eff} measurements for all galaxies in the RESOLVE sample. For this task we employ GALFIT (Peng et al. 2002) to deconvolve the seeing point spread function (PSF) and to perform one

and two component fits on each galaxy. Deconvolution is especially important since the smallest galaxies in RESOLVE are most effected by seeing, and accurate radii measurements are crucial for the study of these objects.

GALFIT needs the following input files to function correctly: an initial input file, an image of the galaxy, a PSF image, an image mask, and a constraint file. We obtain/construct these items as follows:

The initial input file: The initial input file gives GALFIT the files paths to the image, PSF, mask, and constraint file, and also holds the initial guesses for our fit parameters. For the one component fits, we set up our input file to have a section for measuring the level of the sky background, and another section for fitting a Sérsic profile to galaxy. The Sérsic model will find a best fit for the following parameters: central x & y position of the model, integrated magnitude, R_{eff}, Sérsic n, axial ratio (b/a), and position angle. These initial values for these parameters can just be rough guesses, but for our purposes, we use values for the magnitude, R_{eff}, b/a, and PA that are derived from RESOLVE's photometric data (see § 3.1 for more details)

Imaging data: We use publicly-available high resolution Y-band imaging from the UKIDSS Large Area Survey (Lawrence et al. 2007). This data set was chosen because it covers both RESOLVE-A and RESOLVE-B and offers $\sim 0.8''$ seeing resolution corresponding to ~ 350pc at RESOLVE distances in turn letting us span down to the sizes of cE-like galaxies. The Y band is advantageous too, since it probes the underlying stellar population and will not skew our measurements to larger radii if the galaxy is currently experiencing a starburst. We download $\sim 10' \times 10'$ images of each galaxy from the WFCAM Science Archive[1]. While GALFIT does not require images this large to operate normally, we choose this size so that there will be more stars in the field of view which is useful for constructing a PSF. There are only 24 galaxies in RESOLVE that do not have UKIDSS imaging and thus are excluded from our analysis.

The PSF image: GALFIT uses the PSF image to deconvolve the galaxy light profile from the seeing, thereby removing the effects of atmospheric scattering of the galaxy light as the data was taken. We build our PSF image via the following steps.

1. We begin by running Source Extractor on the image to identify every object in the frame, including stars, galaxies, and even sometimes hot pixels. Source Extractor outputs a text file that has estimates of each object's flux, elongation, ellipticity, radius, and `class_star`.

2. With this information, we select stars to use for building our PSF. The limiting parameters are (1) that the flux must be between $5,000 - 100,000$ counts to ensure no extremely faint or saturated stars are included, (2) that the ellipticity be lt 0.2 to ensure we are selecting round objects, (3) that the effective radius of the star be greater than 1

pixel to avoid selecting hot pixels, and (4) that `class_star` is greater than 0.6 to ensure the objects we're picking are most likely stars. We also make sure the stars are not near the image edges, since there can sometimes be image artifacts there. Lastly, we make sure to not include the galaxy we are going to fit, since the cE-like galaxies can sometimes appear to be stars.

3. We next make 101×101 pixel cutouts of each object detected, with the flux peak at pixel $x = 51, y = 51$.

4. Background subtraction is then performed by taking the median of the entire cutout and then subtracting each pixel by this median value.

5. We then reject any of the cutouts that have a background median value greater than 2σ from the mean of the background median values for every cutout. This ensures we are not including any cutouts that have stars with large or bright neighboring objects. We are now left with background-subtracted cutouts of stars with no neighbors that could affect our stacking.

6. Before we can combine all the cutouts, we must normalize the flux of each central star to the same amplitude. To do this, we run each cutout through Source Extractor once more to obtain the fluxes of each central star and use these to weight the cutouts accordingly. We calculate the weight for each cutout as follows: (1) we find the central star with the highest flux of all the cutouts and then (2) divide every flux by this maximum flux. We then divide each cutout by its corresponding weight, which makes each central star have the same amplitude.

7. We then take the median of all the weighted cutouts to create a semi-complete PSF.

8. Lastly, we normalize the semi-complete PSF from Step 7 by dividing each pixel in the frame by the total flux in the image. We find the total image flux by taking the mean of each pixel and multiplying that by the number of pixels in the image (so, 101×101). This ensures that the final PSF image is normalized, i.e., the sum of the flux in each pixel of the cutout would equal one.

Our last step is to fit a 2D Gaussian to the PSF to determine a rough estimate seeing full width half max (FWHM), as a sanity check. We find that the average FWHM for all PSFs is $\sim 0.9''$, only slightly worse than the $\sim 0.8''$ seeing expected for UKIDSS imaging.

The mask image: GALFIT uses the mask image to ignore any objects neighboring our galaxy while it is completing the fit.The first step in making the mask is to create an image that has the same dimensions as our input image but with each pixel value equaling zero. We again use Source Extractor to compile a list of all the objects in the input image, and use this list to replace the pixel values at the coordinates of the located objects with one.

The constant file: The constraint file hosts the limits we are willing to accept for each of the fit parameters. The

constraints for x & y position in the image, integrated magnitude, R_{eff}, Sérsic n, axial ratio (b/a), and position angle for the one component fits are listed in Table 1. We change the constraint file for the two component fits later in the analysis.

parameter	constaint
x & y position	±5 pixels from input value
integrated magnitude	0 – 40
R_{eff}	0.2 – 750 pixels
Sérsic n	0.1 – 8
axial ratio	0 – 1
position angle	-360 – 360

Table 1
Summary of the constraints imposed on our GALFIT models for our initial one component fits for the entire RESOLVE sample.

We use all of the above to obtain a one component, seeing-deconvolved fit for every galaxy in the RESOLVE survey. We then perform the two component fits as follows. We use the output of the one component fit as the basis of the input file for the two component fit. The first two sections in the two component fit initial input file will be identical to the output of the one component fit (except that the names of the files to be output are changed). We then add a third section to include a second Sérsic fit, and change the initial guess for R_{eff} to be double that of the one component best fit. This gives GALFIT an idea to fit on both a core and envelope. The PSF, image, and mask image will all be the same as before. We add to the constraint file the same constraints as listed in Table 1, but for the third section. In other words, there will be two sets of constraints in the file now, with the first set applying to the first Sérsic fit and the second set applying the second Sérsic fit. The constraints for each parameter are the same for both sets. We do not further constrain the two component fits since we are looking for general fits to the wide variety of galaxies in RESOLVE and do not want to over constrain our fits.

For both the one and two component fits, GALFIT outputs a text file with the best fits for central x & y position of the model, integrated magnitude, R_{eff}, Sérsic n, axial ratio (b/a), and position angle and a χ^2/ν as well as a fits file that contains the data, best fit model, and residual images. See Figure 1 for example one and two component fits for a RESOLVE galaxy.

2.3.2. *Selection of CCGs*

Now that we have seeing-deconvolved R_{eff} values for the entire RESOLVE sample, we begin our search for compact core galaxies. We use the AIMSS sample to select a maximum cutoff core-only radius for CCGs at 800 pc. This upper limit ensures that we are selecting the most compact galaxies in RESOLVE, but also lets us select a range of CSSs, including cEs and dEs. RESOLVE's lower stellar mass limit of restricts us from reaching down to UCD masses.

We start our search for CCGs by using the one component fit from the above analysis and select galaxies with R_{eff} values < 1000 pc. Since we are looking for galaxies with compact cores, going up to $R_{eff} \sim 1000$ pc allows us to select objects with cores that are dominating the light and therefore may have a smaller core R_{eff} in a two component fit. We also limit the χ^2/ν to be < 1.3, since values above this represent galaxies with large residuals left over, which are normally spirals

or irregulars that we would not consider a CCG. After this selection, we are left with 124 galaxies in the CCG candidate sample.

Next, we perform new two component fits using different fitting constraints: (1) the central x and y positions are taken from the one component fit and are held constant for both Sérsic components, (2) the R_{eff} of the second Sérsic fit is constrained to always be larger than that of the first Sérsic fit, and (3) the Sérsic n of the second component is held constant at 1 for an exponentially decreasing disk profile. We let the values of R_{eff}, the integrated magnitude, b/a ratio, and PA change for both fits. By doing this, we are forcing GALFIT to fit on a core (the first Sérsic fit) and disky envelope (the second Sérsic fit) for each CCG candidate.

We then examine the fits by eye and create our final CCG sample by selecting where the core $R_{eff} < 800$ pc and $\chi^2/\nu < 1.3$ to again exclude poor fits. Our sample is thus comprised of 96 CCGs in total (63 from RESOLVE-A and 33 from RESOLVE-B). This represents $\sim 6\%$ of the total RE-SOLVE galaxy sample. Figure 3 shows their distribution in stellar mass and decomposed R_{eff} compared to other RE-SOLVE galaxies and the AIMSS cEs and dEs. For the RE-SOLVE sample, we are plotting the one component fits, while for the CCGs, we are plotting the core R_{eff} from the fixed two component fits.

We quantify the amount of light in the core vs. the envelope by taking a ratio of the fluxes of the core and the envelope. The flux of each component is computed with $m = -2.5 \times \log(flux)$, where m is the integrated magnitude output from GALFIT. For each plot in this paper, we color code the CCGs by the logarithm of the flux ratio. CCGs with more light in the envelope will have log(flux ratio) < 0, and will hereafter be called "envelope-dominated' CCGs. CCGs with more light in the core will have log(flux ratio) > 0, and will hereafter be called "core-dominated" CCGs. CCGs with log(flux ratio) ~ 0 will have both a bright core plus an extended envelope, and will be called "core+envelope" CCGs. See Figure 2 for examples of CCGs on this continuous scale. There are some cases when GALFIT cannot find a core or an envelope, and will instead fit an extremely large and faint component instead. Where this happens (5 out of 96 cases), we classify this fit as either all core/envelope depending on which component was bad (log(flux ratio) = -1 or 1). We also see in 4 out of the 96 cases that the R_{eff} values for each component will be exactly the same value to 3-4 decimal points, indicating a probable bad fit for one component. When this occurs, we classify the galaxy as being all core (log(flux ratio) = 1).

We see in Figure 3 that both core- and envelope-dominated CCGs tend to be at the higher end of the R_{eff} values, while core+envelope CCGs tend to be the lower R_{eff} values. There also are more core-dominated CCGs at the higher $M_\star$ end while envelope-dominated CCGs tend to reside at low $M_\star$.

3. METHODS

3.1. *Photometry: galaxy colors, stellar and baryonic masses, and star formation rates*

The RESOLVE survey overlaps with a number of photometric surveys, including GALEX *NUV* (Morrissey et al. 2007), SDSS-DR8 *ugriz* (Aihara et al. 2011), and UKIDSS *YHK* and/or 2MASS *JHK* (Skrutskie et al. 2006). We reprocess this photometric data to improve upon the standard SDSS data pipeline, as described in detail in Eckert et al. (2015). The

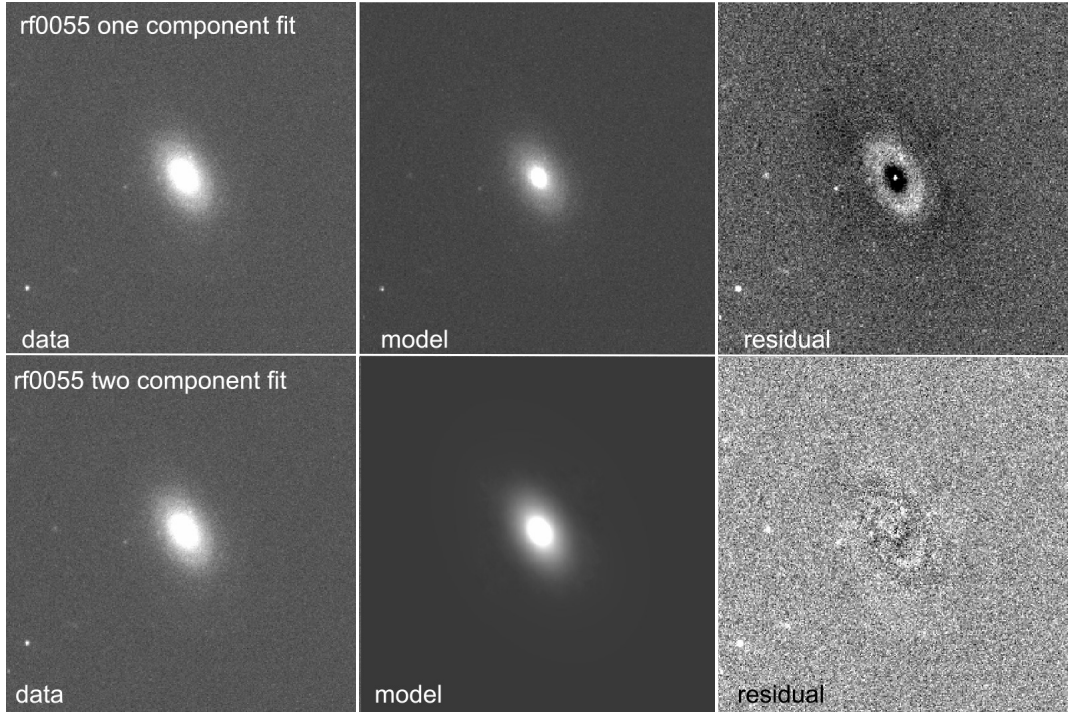**Figure 1.**

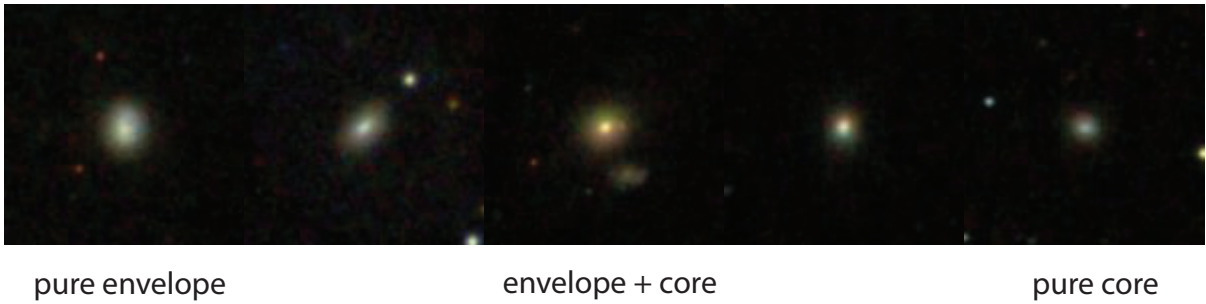pure envelope   envelope + core   pure core

Figure 2. Five of the 96 CCGs in the final sample arranged in order from envelope-only to envelope+core to core-only. Images are taken from the SDSS-DR8 image list tool. The central image is rf0492, a CCG with possible ram pressure stripping origins (see § 4.3).

main differences in this processing are (1) improved sky subtraction following Blanton et al. (2011) for SDSS photometry plus custom background subtraction for UKIDSS/2MASS, (2) the definition of elliptical apertures on the sum of the higher S/N *gri* images to determine the PA and b/a ratio of the outer disk (if present), and (3) the application of the same apertures to all bands which allows us to measure magnitudes for galaxies that may not have been detected by automated survey pipelines, especially low surface brightness galaxies in 2MASS, UKIDSS, and GALEX. Then, total magnitudes are derived for each band using an exponential outer disk fit method, curve of growth method, or color correction method (see Figure 2 in Eckert et al. (2015)).

Colors, stellar masses and fractional stellar mass growth rates (FSMGR) are then derived from these *NUVugrizYJHK* magnitudes using the spectral energy distribution (SED) modeling code described in Kannappan & Gawiser (2007), Kannappan et al. (2009), and Kannappan et al. (2013). FSMGR is similar to a star formation rate, but it instead gives the ratio of stellar mass created in the last Gyr to the stellar mass previously existing. Therefore, an FSMGR of 1 means that the galaxy has doubled its stellar mass in the last Gyr.

The HI masses for RESOLVE are from the blind 21cm ALFALFA survey (Haynes et al. 2011) and from new pointed observations with the GBT and Arecibo telescopes (Stark et al. in prep.). We use these masses along with the stellar masses computed in the SED models to estimate baryonic masses.

3.2. *Environmental Metrics*

RESOLVE is advantageous to this study because it offers excellent environment information, allowing us to search for CCGs in all environments including groups, clusters, walls, and filaments. We explore the environments of CCGs using two different metrics: the mass of their group halo and their distance to another galaxy. The group halo mass allows us to look for CCGs that are M32–Andromeda analogs where tidal stripping may be at play, or conversely look for CCGs in large groups where ram-pressure stripping could occur. The distance to neighboring galaxies lets us examine if interaction may occur or look for analogs of the isolated galaxies found by Huxor et al. (2013) and Paudel et al. (2014).

Galaxy groups are identified using the friends-of-friends algorithm of Berlind et al. (2006), and the masses of these group halos are calculated based on the observed total *r*-band luminosity of galaxies in each group using abundance matching, as described in Blanton & Berlind (2007). More information on group identification can be found in Moffett et al. (2015). The nearest neighbor distances are computed using the RA, Dec, and redshifts of each galaxy and along with spherical geometry principles.

3.3. *Kinematics*

3.3.1. *SOAR spectroscopy*

The RESOLVE survey gets the bulk of its spectroscopic data from the SOuthern Astrophysical Research (SOAR) Telescope, located at Cerro Tololo, Chile. We employ the Goodman Spectrograph, designed and built by UNC, along with RESOLVE's custom-built image slicer with 3 $1''$ slits to observe galaxies in both a broad setup and either an emission- or absorption-line kinematic setup. With this absorption-line setup, we are able to derive velocity dispersions. We use the highly-efficient 2100 l/mm VPH grating in order to cover a wavelength range 4858-5503Å, which includes stellar absorption lines such as Hβ, the magnesium triplet, and Fe5270/5335. To achieve S/N $\sim$ 25 per Å, we bin each central spectrum to R$_{\text{eff}}$.

The reduction process is as follows: we use standard IRAF tasks to perform bias and overscan subtraction, trimming of the science data to remove unnecessary spatial coverage, and flat fielding. We then use LA_COSMIC (van Dokkum 2001) to clean cosmic rays from each science exposure. We next complete a wavelength calibration and transformation, and then perform object tracing and extraction into a 1D spectrum using the IRAF task apall. We lastly combine the individual exposures using the IRAF task scombine.

3.3.2. *Gemini-South spectroscopy*

A subset of the faintest or smallest galaxies in RESOLVE are observed with the Gemini-South IFU for their kinematics instead of SOAR. For this absorption-line setup, we use the B1200 grating in 1-slit mode to cover a spatial region of $3'' \times 5''$ and the spectral range 4200-5600Å. The B1200 grating offers 0.9Å resolution when binned spectrally by 2. We calculate our exposure times such that we achieve S/N $\sim$ 25 per Å after binning by 2 in the spectral direction and summing the fibers out to R$_{\text{eff}}$.

The spectral reduction proceeds as follows. Using the standard IRAF Gemini-GMOS data packages, bias and overscan subtraction, spatial trimming, flat fielding and fiber identification are performed. We next use the GMOS package gemCRspec, a wrapper for LA_COSMIC, to clean cosmic rays from each science exposure. We then correct the science frames for quantum efficiency differences between CCDs. Wavelength transformation, sky subtraction, and flux calibration are subsequently performed, and lastly, data cubes are made and summed. We then stack the individual fiber spectra out to R$_{\text{eff}}$ to create a 1D spectrum for each galaxy that has S/N $\sim$ 25. More information on the data reduction for the Gemini GMOS IFU can be found in § 6.2.

3.3.3. *Velocity Dispersion Extraction*

We then derive σ from the both the SOAR and Gemini spectra using PPXF, the penalized pixel fitting code from Cappellari & Emsellem (2004). This code fits a combination of high-resolution (FWHM = 0.55 Å) ELODIE-based model spectra from Maraston & Strömbäck (2011) to the observed input spectrum, and determines a best fit solution for σ. A caveat to these fits is that they are not corrected for any stellar rotation, which will make absorption lines wider and thus skews the derived σ values toward higher values depending on the amount of rotation in each galaxy. Future work will include implementing a stellar rotation subtraction routine for these fits, but preliminary testing by binning the spectra to $1''$ instead of to R$_{\text{eff}}$ shows little change between the derived σ values.

4. RESULTS

4.1. *Colors and Star formation rates*

We begin by examining the colors of the CCG sample. The left side of Figure 6 shows the $u-r$ colors of our CCG sample plotted against M$_\star$, compared to the RESOLVE sample as a whole. An unusual finding is that many CCGs live on the blue sequence, since most CSSs are typically thought of as being "red and dead". The right side of Figure 6 shows FSMGR vs. M$_{\text{bary}}$ for the same objects. As with the colors, we find that many CCGs are forming stars at a rapid rate (FSMGR
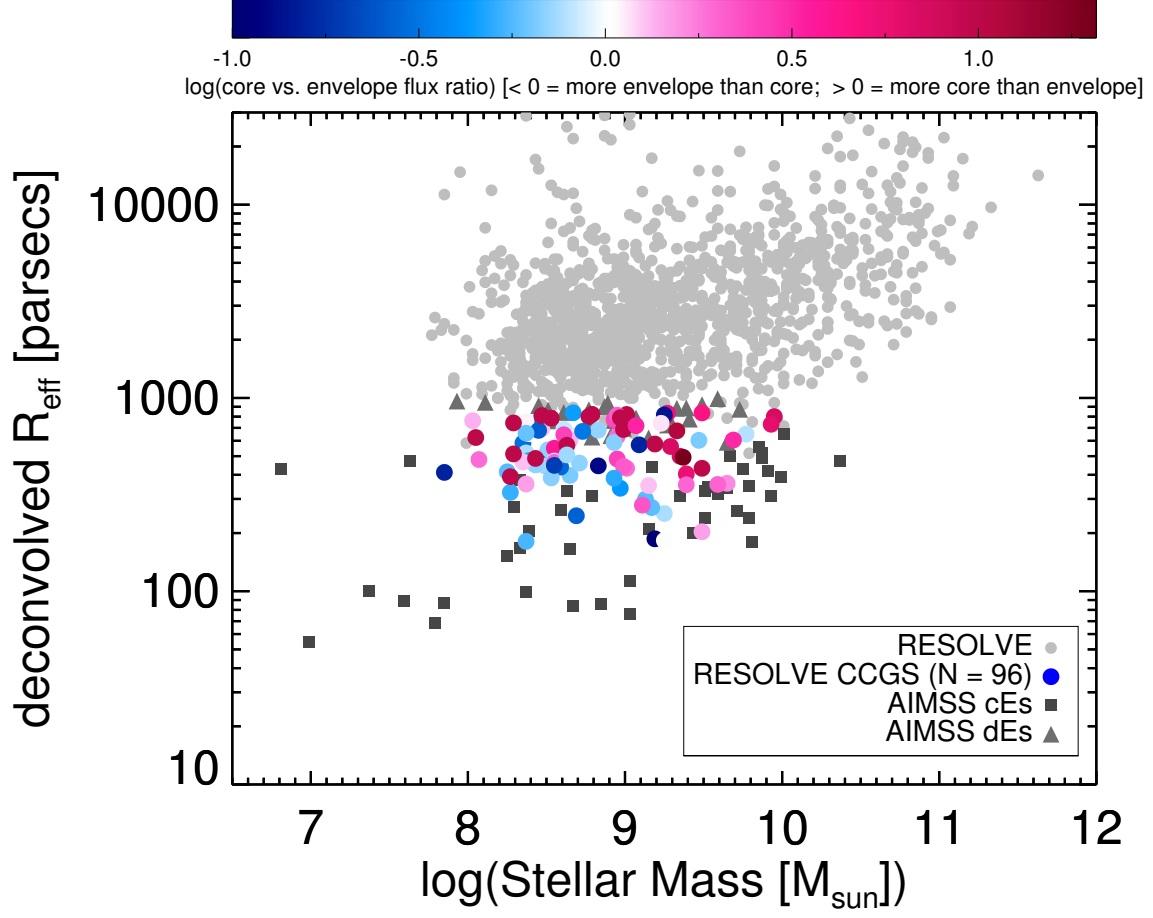
Figure 3. We plot here the deconvolved R_{eff} measurements for the entire RESOLVE sample, along with the CCSs of the AIMSS catalog. In grey are the RESOLVE (non-CCG) galaxies, which are plotted using their one component fit R_{eff}. The CCG sample is using the core R_{eff} of the two component fits, which is why they may appear separated from the full RESOLVE sample. The colors of the CCGs represent the logarithm of the flux ratio between the core and envelope. Galaxies with log(flux ratio) near 0 will have both a core and envelope, while galaxies with log(flux ratio) $\sim \pm 1$ will have more light in the core (+1) or envelope (-1).
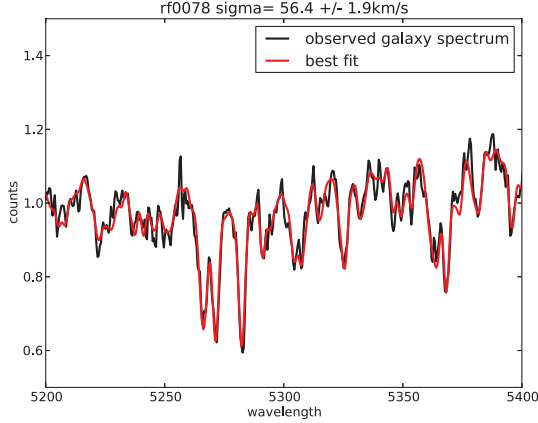
Figure 4. Plotted here in black is a summed Gemini-South IFU spectrum for the CCG rf0078. Overplotted in red is the pPXF best fit model spectrum. The spectrum is zoomed-in to show the MgB triplet fit at ~ 5275 Å.

~ 1 means that the galaxy has doubled its mass in the last Gyr), again an unexpected finding which could indicate that some CCGs are still in the process of forming (if dissipatively formed) or relaxing (if a tidally-stripped remnant).

Looking now at the log(flux ratio values), we see that red sequence CCGs tend to be more core-dominated, while blue sequence CCGs tend to me more envelope-dominated. There also tends to be more core-dominated CCGs at lower FS-MGR, while envelope-dominated CCGs reside at higher FS-MGR. There is considerable scatter though, making these trends harder to qualify.

4.2. *Environments*

We investigate the distribution of CCGs throughout the cosmic web, and find that CCGs span a range of different environments (see Figure 6). We see many CCGs residing in low mass groups, similar to the M32–Andromeda relationship, which suggests that tidal stripping could be at play. On the opposite end, we see several CCGs in massive group halos, and that these tend to be either core- or envelope dominated CCGs. This hints towards ram pressure stripping being at play in these environments, especially for those CCGs at larger distances from other galaxies. There are also many CCGs that are > 1 Mpc away from another object in RA–Dec–redshift space, resembling the isolated cEs found by Huxor et al. (2013) and Paudel et al. (2014), which may point to a dissipative formation scenario since there is no nearby object to have performed the stripping.

4.3. *Kinematics*

We lastly investigate the kinematics of the CCG sample using the σs derived from SOAR and Gemini telescope data. Figure 7 plots the σ-$M_\star$ relation for the 8 CCGs with σ measurements along with the other 80+ RESOLVE galaxies with measured σs. Galaxies with σ offset to higher values point to tidal stripping occurring, since they will have more Conversely, σs that lie on the trend may point dissipative formation occurring, since these will have formed similarly to normal elliptical galaxies.

We find that most of the CCGs tend to follow the dissipative formation track. However, there is one CCG with a core+envelope that lies close to M32, a tidally stripped cE, in

the relation. We now take a closer look at this CCG, rf0492. This CCG lives on the red sequence, has an FSMGR~ 0.08, and has a prominent core, and can be seen in the center image of Figure 2. Its nearest 3D neighbor is 2.63 Mpc away, making it fairly isolated, even though it lives in a group with halo mass $= 10^{12.09}$ M$_\odot$. This could be an example of a CCG that was perturbed, perhaps even ram pressure stripped, as it fell into this larger group, causing gas to funnel to the center to create the core we see.

5. SUMMARY

In this paper we have examined the colors, FSMGR, environments, and kinematics of the 96 compact core galaxies (CCGs) in the RESOLVE survey. We have selected CCGs to have a seeing-deconvolved, core-only $R_{\rm eff} < 800$ pc, based on the sizes of the compact and dwarf ellipticals in the AIMSS catalog. We have quantified the amount of light in the cores and envelopes of each CCG by performing two component fits with GALFIT and taking the logarithm of the ratio of the fluxes of the two different components. CCGs with more light in the envelope have log(flux ratio) < 0 and are called "envelope-dominated' CCGs. CCGs with more light in the core have log(flux ratio) > 0 and are called "core-dominated" CCGs. CCGs with log(flux ratio) ~ 0 have both a bright core plus an extended envelope and are called "core+envelope" CCGs. Our main results can be summarized as follows:

1. Figure 3 shows that both core- and envelope-dominated CCGs tend to be at the higher end of the $R_{\rm eff}$ values, while core+envelope CCGs tend to be the lower $R_{\rm eff}$ values. There also are more core-dominated CCGs at the higher $M_\star$ end while envelope-dominated CCGs tend to reside at low $M_\star$.

2. We find that many CCGs live on the blue sequence and are forming stars at a rapid rate (see Figure 5), which could indicate that some CCGs are still in the process of forming (if dissipatively formed) or relaxing (if a tidally-stripped remnant).

3. We find that CCGs span a range of different environments (see Figure 6). Many CCGs live in low mass groups, similar to the M32–Andromeda relationship, perhaps hinting at tidal stripping formation scenarios. Others live in massive group halos and tend to be either core- or envelope dominated CCGs, conversely hinting towards ram pressure stripping being at play. There are also many CCGs that are > 1 Mpc away from another object in RA–Dec–redshift space, resembling the isolated cEs found by Huxor et al. (2013) and Paudel et al. (2014), which may point to a dissipative formation scenario.

4. Using velocity dispersions (σ) derived from the SOAR and Gemini telescopes, we look for offsets in σ-$M_\star$ relation that could point to tidal stripping or dissipative formation scenarios (see Figure 7). We find that CCGs tend to follow the dissipative formation track, however one CCG with a core+envelope lies close to M32, a tidally stripped cE, in the relation.
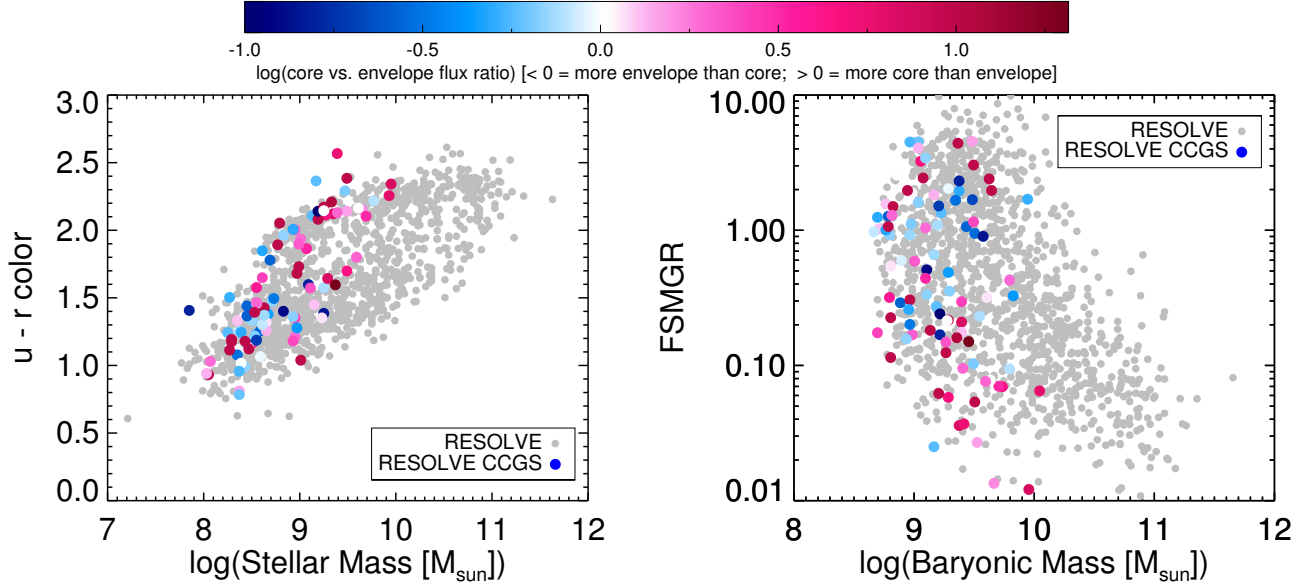
6. FUTURE WORK

6.1. *Gas Content*

Figure 5. **(a.)** On the left we plot the $u-r$ colors against stellar mass of CCGs with the entire RESOLVE sample. **(b.)** On the right we have plotted the FSMGR against baryonic mass for both the CCGs and entire RESOLVE sample.

The amount of neutral Hydrogen gas a CCG has may be able to give us insights into its evolution over time. For example, a CCG in a galaxy cluster with little HI gas may point towards ram pressure stripping being important. Combined with CCG colors and FSMGR, the gas content may be an important tool in determining the evolution of a CCG.

6.2. *Metallicities*

Janz et al. (2015) have shown that tidally-stripped CSSs are systematically offset to higher metal abundances. With the SOAR data we have in hand, we may be able to test this hypothesis for the CCG sample and use this method as another way to discern formation scenarios.

REFERENCES

Aihara, H., Allende Prieto, C., An, D., et al. 2011, The Astrophysical Journal Supplement Series, 193, 29

Bekki, K., Couch, W. J., & Drinkwater, M. J. 2001, The Astrophysical Journal, 552, L105

Bekki, K., & Freeman, K. C. 2003, Monthly Notices of the Royal Astronomical Society, 346, L11

Berlind, A. A., Frieman, J., Weinberg, D. H., et al. 2006, The Astrophysical Journal Supplement Series, 167, 1

Bertin, E., & Arnouts, S. 1996, Astronomy and Astrophysics Supplement Series, 117, 393

Blanton, M. R., & Berlind, A. A. 2007, The Astrophysical Journal, 664, 791

Cappellari, M., & Emsellem, E. 2004, Publications of the Astronomical Society of the Pacific, 116, 138

Chilingarian, I., Cayatte, V., Revaz, Y., et al. 2009, Science (New York, N.Y.), 326, 1379

Chilingarian, I., & Zolotukhin, I. 2015, Science (New York, N.Y.), 348, 418

Chilingarian, I. V., & Bergond, G. 2010, Monthly Notices of the Royal Astronomical Society: Letters, 405, L11

Chilingarian, I. V., Sil'chenko, O. K., Afanasiev, V. L., & Prugniel, P. 2007, Astronomy Letters, 33, 292

Choi, P. I., Guhathakurta, P., & Johnston, K. V. 2002, The Astronomical Journal, 124, 310

Colless, M., Dalton, G., Maddox, S., et al. 2001, Monthly Notices of the Royal Astronomical Society, 328, 1039

Crawford, S. M., Wirth, G. D., Bershady, M. A., & Randriamampandry, S. M. 2016, The Astrophysical Journal, 817, 87

Crnojević, D., Ferguson, A. M. N., Irwin, M. J., et al. 2014, Monthly Notices of the Royal Astronomical Society, 445, 3862

Drinkwater, M. J., Jones, J. B., Gregg, M. D., & Phillipps, S. 2000, Publications of the Astronomical Society of Australia, 17, 227

Driver, S. P., Hill, D. T., Kelvin, L. S., et al. 2011, Monthly Notices of the Royal Astronomical Society, 413, 971

Eckert, K. D., Kannappan, S. J., Stark, D. V., et al. 2015, The Astrophysical Journal, 810, 166

Eckert, Â., Kannappan, Â., Stark, Â., et al. 2016, eprint arXiv:1604.03957

Evstigneeva, E. A., Drinkwater, M. J., Jurek, R., et al. 2007, Monthly Notices of the Royal Astronomical Society, 378, 1036

Faber, S. M. 1973, The Astrophysical Journal, 179, 423

Falco, E., Kurtz, M., Geller, M., et al. 1999, Publications of the Astronomical Society of the Pacific, 111, 438

Forbes, D. A., Norris, M. A., Strader, J., et al. 2014, Monthly Notices of the Royal Astronomical Society, 444, 2993

Graham, A. W. 2002, The Astrophysical Journal, 568, L13

Guzmán, R., Koo, D. C., Faber, S. M., et al. 1996, The Astrophysical Journal, 460, doi:10.1086/309966

Hau, G. K. T., Spitler, L. R., Forbes, D. A., et al. 2009, Monthly Notices of the Royal Astronomical Society: Letters, 394, L97

Haynes, M. P., Giovanelli, R., Martin, A. M., et al. 2011, The Astronomical Journal, 142, 170

Haşegan, M., Jordan, A., Cote, P., et al. 2005, The Astrophysical Journal, 627, 203

Huxor, A. P., Phillipps, S., & Price, J. 2013, Monthly Notices of the Royal Astronomical Society, 430, 1956

Huxor, A. P., Phillipps, S., Price, J., & Harniman, R. 2011, Monthly Notices of the Royal Astronomical Society, 414, 3557

Janz, J., Norris, M. A., Forbes, D. A., et al. 2015, Monthly Notices of the Royal Astronomical Society, 456, 617

Jennings, Z. G., Romanowsky, A. J., Brodie, J. P., et al. 2015, The Astrophysical Journal, 812, L10

Jones, D. H., Read, M. A., Saunders, W., et al. 2009, Monthly Notices of the Royal Astronomical Society, 399, 683

Jones, J. B., Drinkwater, M. J., Jurek, R., et al. 2006, The Astronomical Journal, 131, 312

Kannappan, S. J., & Gawiser, E. 2007, The Astrophysical Journal, 657, L5

Kannappan, S. J., Guie, J. M., & Baker, A. J. 2009, The Astronomical Journal, 138, 579

Kannappan, S. J., Stark, D. V., Eckert, K. D., et al. 2013, The Astrophysical Journal, 777, 42

Koo, D. C., Bershady, M. A., Wirth, G. D., Stanford, S. A., & Majewski, S. R. 1994, The Astrophysical Journal, 427, L9

Kormendy, J., & Bender, R. 2012, The Astrophysical Journal Supplement Series, 198, 2

Kormendy, J., Bender, R., Magorrian, J., et al. 1997, The Astrophysical Journal, 482, L139
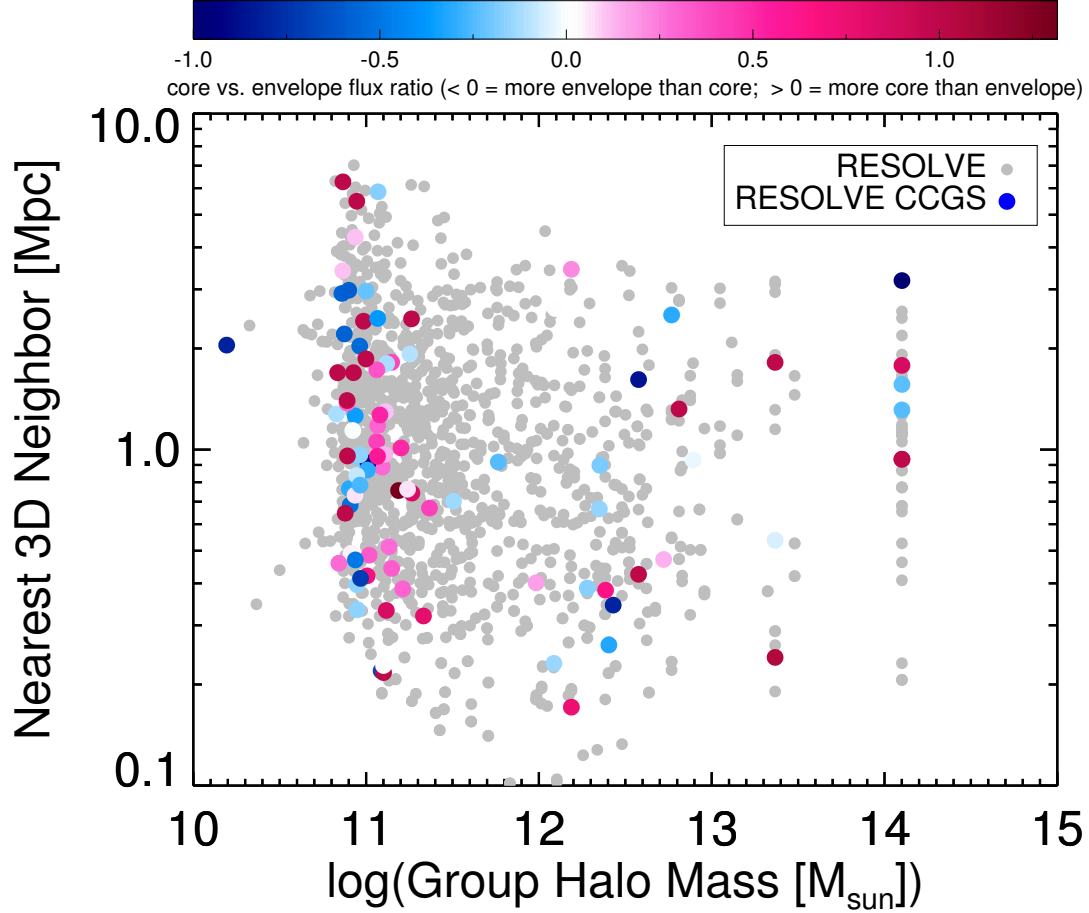
Figure 6. We plot here the group halo mass against the nearest 3D neighbor for the RESOLVE survey and CCG sample. We see that CCGs live in a variety of environments, from extremely isolated (nearest neighbor > 1 Mpc) to massive ($M_{halo} \sim 10^{13}$ $M_{\odot}$) groups. There is no obvious trend into whether cores+envelopes and cores/envelopes preferentially live in different environments.

Lawrence, A., Warren, S. J., Almaini, O., et al. 2007, Monthly Notices of the Royal Astronomical Society, 379, 1599

Liu, C., Peng, E. W., Côté, P., et al. 2015, The Astrophysical Journal, 812, 34

Madrid, J. P., Graham, A. W., Harris, W. E., et al. 2010, The Astrophysical Journal, 722, 1707

Maraston, C., & Strömbäck, G. 2011, Monthly Notices of the Royal Astronomical Society, 418, 2785

Mieske, S., Hilker, M., & Infante, L. 2002, Astronomy and Astrophysics, 383, 823

Mieske, S., Hilker, M., Misgeld, I., et al. 2009, Astronomy and Astrophysics, 498, 705

Misgeld, I., Mieske, S., & Hilker, M. 2008, Astronomy and Astrophysics, 486, 697

Moffett, A. J., Kannappan, S. J., Berlind, A. A., et al. 2015, The Astrophysical Journal, 812, 89

Morrissey, P., Conrow, T., Barlow, T. A., et al. 2007, The Astrophysical Journal Supplement Series, 173, 682

Norris, M. A., & Kannappan, S. J. 2011, Monthly Notices of the Royal Astronomical Society, 414, 739

Norris, M. A., Kannappan, S. J., Forbes, D. A., et al. 2014, Monthly Notices of the Royal Astronomical Society, 443, 1151

Paturel, G., Petit, C., Prugniel, P., et al. 2003, Astronomy and Astrophysics, 412, 45

Paudel, S., Lisker, T., Hansson, K. S. A., & Huxor, A. P. 2014, Monthly Notices of the Royal Astronomical Society, 443, 446

Peng, C. Y., Ho, L. C., Impey, C. D., & Rix, H.-W. 2002, The Astronomical Journal, 124, 266

Penny, S. J., Forbes, D. A., Pimbblet, K. A., & Floyd, D. J. E. 2014, Monthly Notices of the Royal Astronomical Society, 443, 3381

Pfeffer, J., & Baumgardt, H. 2013, Monthly Notices of the Royal Astronomical Society, 433, 1997

Phillipps, S., Drinkwater, M. J., Gregg, M. D., & Jones, J. B. 2001, The Astrophysical Journal, 560, 201

Price, J., Phillipps, S., Huxor, A., et al. 2009, Monthly Notices of the Royal Astronomical Society, 397, 1816

Seth, A. C., van den Bosch, R., Mieske, S., et al. 2014, Nature, 513, 398

Skrutskie, M. F., Cutri, R. M., Stiening, R., et al. 2006, The Astronomical Journal, 131, 1163

Smith Castelli, A. V., Cellone, S. A., Faifer, F. R., et al. 2012, Monthly Notices of the Royal Astronomical Society, 419, 2472

Smith Castelli, A. V., Faifer, F. R., Richtler, T., & Bassino, L. P. 2008, Monthly Notices of the Royal Astronomical Society, 391, 685

vanÂ&Dokkum, P. 2001, Publications of the Astronomical Society of the Pacific, 113, 1420

Wehner, E. M. H., & Harris, W. E. 2007, The Astrophysical Journal, 668, L35

York, D. G., Adelman, J., Anderson, Jr., J. E., et al. 2000, The Astronomical Journal, 120, 1579

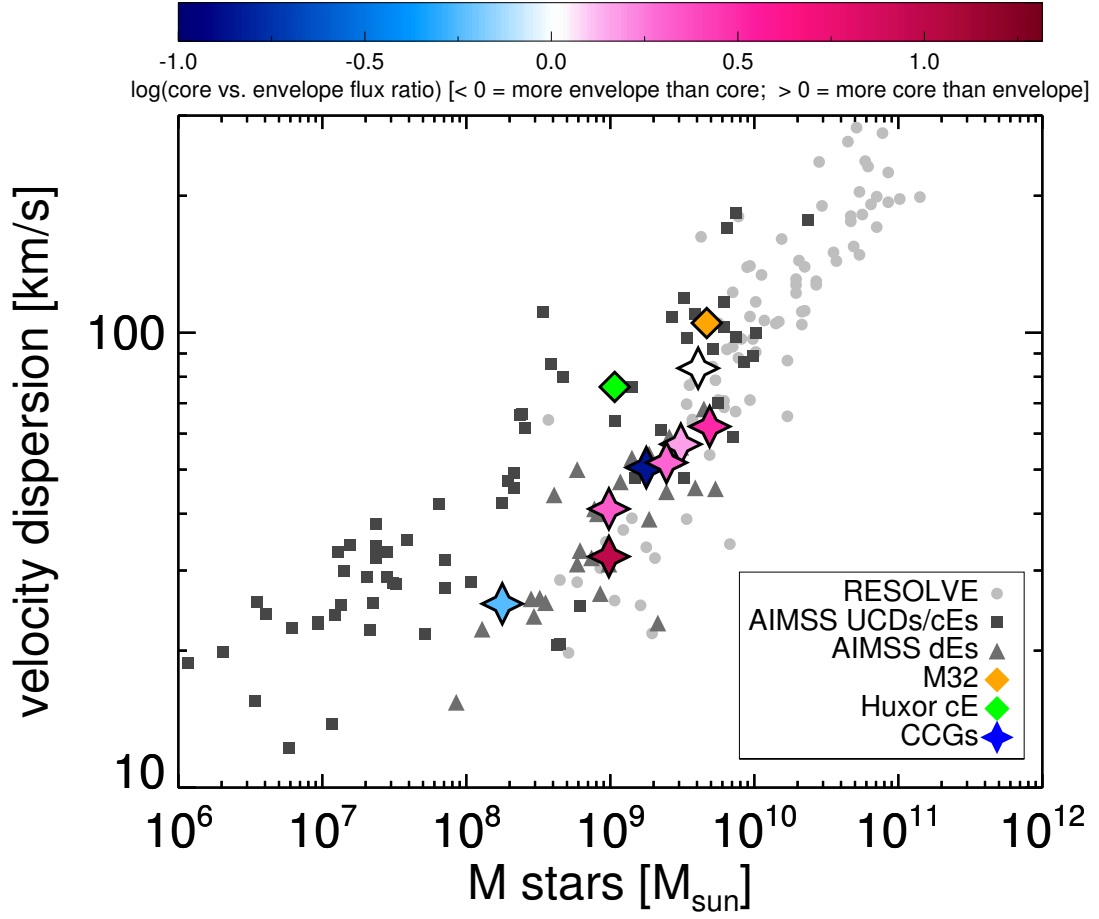Zhang, H.-X., Peng, E. W., Côté, P., et al. 2015, The Astrophysical Journal, 802, 30

APPENDIX

Figure 7. Here we plot the stellar mass vs. velocity dispersion (σ) for the RESOLVE sample, CCGs, and the CSSs of the AIMSS catalog. Most CCGs appear to be following the dissipative formation track.